J. Fluid Mech. (1988), *vol.* 195, *pp.* 495–522
Printed in Great Britain

Modulated and unmodulated travelling azimuthal waves on the toroidal vortices in a spherical Couette system

By KOICHI NAKABAYASHI AND YOICHI TSUCHIDA
Department of Mechanical Engineering, Nagoya Institute of Technology, Nagoya 466, Japan

(Received 2 October 1987)

We have investigated the modulated and unmodulated travelling azimuthal waves appearing on the toroidal Taylor–Görtler (TG) vortices in a fluid contained between two concentric spheres with the inner sphere rotating. For smaller-clearance cases, toroidal TG vortices appear at the equator, just as in the flow between two concentric cylinders with the inner cylinder rotating. When the Reynolds number of the flow increases quasi-statically, spiral TG vortices appear in addition to toroidal TG vortices, and no modulation occurs, even if the Reynolds number further increases quasi-statically. However, when the Reynolds number is increased from zero to a particular value with a specific acceleration of the inner sphere, modulated wavy toroidal TG vortices appear. We found that the necessary condition for occurrence of modulation is the prevention of spiral TG vortices. Using simultaneous flow-visualization and spectral techniques, and measuring the fluctuation of sinks and sources of vortex boundaries, we obtained the frequency f_1 of travelling azimuthal waves passing a fixed point in the laboratory and the modulation frequencies f_2 and f_2' of these waves, as determined by an observer in the laboratory and an observer fixed in a reference frame that rotates in phase with the travelling azimuthal waves, respectively. The relationship among the characteristic frequencies, f_1, f_2 and f_2', obtained by modal analysis and the experimental results, is $(f_2'+kf_1/m)/f_2 = -1$, where k and m are a modulation parameter and the wavenumber of travelling azimuthal waves, respectively.

1. Introduction

The flow between two concentric spheres with the inner sphere rotating and the outer sphere fixed (spherical Couette flow) for smaller-clearance cases shows the same Taylor instability as that in the flow between two concentric cylinders with the inner cylinder rotating and the outer cylinder fixed (circular Couette flow). Hence, just as Taylor vortices appear for the circular Couette flow (CCF), toroidal Taylor–Görtler (TG) vortices appear near the equator for the spherical Couette flow (SCF), as reported by Sawatzki & Zierep (1970), Munson & Menguturk (1975), Wimmer (1976), Waked & Munson (1978), Nakabayashi (1978, 1983), Krause (1980), Yavorskaya *et al.* (1980), Bartels (1982), Bühler & Zierep (1983, 1984), Dennis & Quartapelle (1984), Schrauf & Krause (1984) and Schrauf (1986).

Since fluid motion corresponds to vortex motion, it is important to investigate vortex motion appearing in the laminar–turbulent transition phenomenon, in order to understand clearly details of the disturbance in the flow. For CCF, a singly periodic velocity fluctuation was found to correspond to the travelling azimuthal

waves on the Taylor vortices by Coles (1965), Fenstermacher, Swinney & Gollub (1979), Mobbs, Preston & Ozogan (1979), Walden & Donnelly (1979), Bouabdallah & Cognet (1980), DiPrima & Swinney (1981) and others. Also, a doubly periodic velocity fluctuation was discovered to correspond to both amplitude- and frequency-modulated travelling azimuthal waves on the Taylor vortices by Swift, Gorman & Swinney (1981), Rand (1981), Gorman & Swinney (1982), and King *et al.* (1984), for example.

For SCF, however, a singly periodic velocity fluctuation corresponds to the spiral TG vortices, and a doubly periodic velocity fluctuation corresponds to a compound combination of the travelling azimuthal waves on toroidal TG vortices and the spiral TG vortices or the shear waves within the Ekman boundary layer, when the Reynolds number is quasi-statically increased from zero, as reported in Nakabayashi & Tsuchida (1988). Thus, for SCF, the vortex structure corresponding to singly or doubly periodic velocity fluctuation is not only different from that for CCF, but also no modulation of the travelling azimuthal waves occurs.

On the other hand, when the Reynolds number is raised from zero to a particular value with a specific acceleration rate, no spiral TG vortices occur, and consequently wavy and modulated wavy toroidal TG vortices appear. Accordingly, a singly periodic velocity fluctuation corresponding to the travelling azimuthal waves and a doubly periodic velocity fluctuation corresponding to both amplitude- and frequency-modulated travelling azimuthal waves can be obtained, just as for CCF. However, there may be differences between SCF and CCF in the characteristic frequencies f_1, f_2 and f_2', because the Ekman boundary layer in SCF influences the travelling azimuthal waves in the wavy and modulated wavy toroidal TG vortex flows. Here f_1 is the frequency of the unmodulated travelling azimuthal waves passing a fixed point of observation in the laboratory, f_2 is the frequency of modulation of the travelling azimuthal waves, as determined by an observer in the laboratory, and f_2' is the modulation frequency as determined by an observer fixed in a reference frame that rotates in phase with the travelling azimuthal waves (rotating frame). Although measurements of f_1, f_2 and f_2' and a modal analysis of travelling azimuthal waves were reported for CCF by Swift *et al.* (1981), Rand (1981), Gorman & Swinney (1982) and King *et al.* (1984), there has been neither measurement nor consideration of the relationship among f_1, f_2 and f_2' for SCF.

In the present study, we investigate the flow states, the characteristic frequencies and the condition for the appearance of the wavy and modulated wavy vortex flows in SCF by simultaneous spectral and flow-visualization measurements, and then undertake the modal analysis of unmodulated and modulated waves. In §2 we describe the experimental techniques. The experimental results and modal analysis of unmodulated waves are described in §3. In §4 the experimental results of modulated waves are presented. The modal analysis of modulated waves is discussed in §5, where the modulation pattern is simulated using a specific function in comparison with the experimental data. Also, the present results of modulated and unmodulated waves are compared with those obtained for CCF. The conclusions are presented in §6.

2. Experimental techniques

In the present experiment, simultaneous spectral and flow-visualization measurements were performed. The experimental apparatus, shown in figure 1,

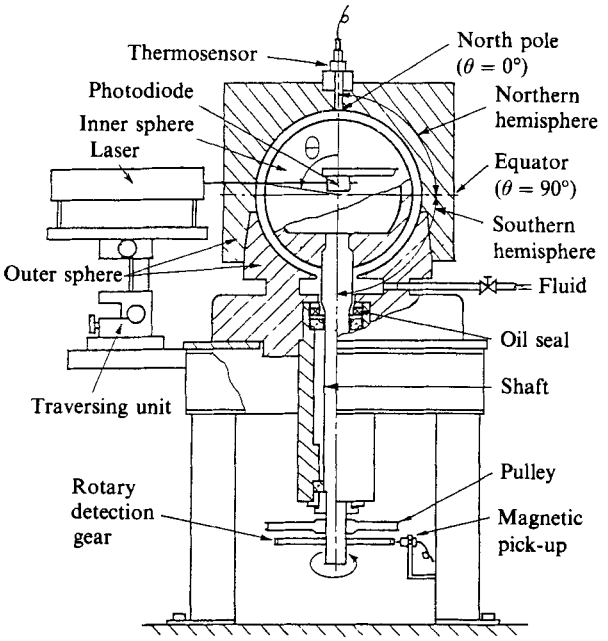

FIGURE 1. Experimental apparatus for simultaneous spectral and flow-visualization measurements by measuring the intensity of laser light scattered by the aluminium flakes.

is the same as that used in an earlier study (Nakabayashi 1983). The radius R_1 of the inner sphere, the radius R_2 of the outer sphere and the clearance ratio β defined as $(R_2-R_1)/R_1$, are 76.89 ± 0.01 mm, 87.53 ± 0.01 mm and 0.138, respectively. And the critical Reynolds number Re_c obtained from flow-visualization measurements was 900. The Reynolds number Re is defined as $2\pi\hat{f}_0 R_1^2/\nu$, where $\hat{f}_0$ is the rotation frequency of the inner sphere, and ν the kinematic viscosity of the fluid. The accuracy of the whip of the rotating inner sphere and the concentricity of the inner and outer spheres were confirmed to be within ±0.015 mm and ±0.01 mm, respectively.

Flow patterns were made visible in the working fluid, Glycerol–water solution of 50% concentration, at room temperature using a suspension of small aluminium flakes that align with the flow direction. In order to clarify the flow state, both the whole spherical surface and the meridian cross-section of the spherical annulus were observed and photographed at fixed intervals over time in the laboratory, where the former was illuminated by front lighting and obtained using mirrors, and the latter was lighted by slit illumination.

The wavenumber m of the travelling azimuthal waves was obtained from photographs of all the waves around the annulus taken simultaneously. The k-value was determined as described in §4. The frequencies f_1 and f_2 in the laboratory were measured using a stop-watch, confirmed by visual observation in real time, and determined simultaneously from the spectral analysis of the intensity of the laser light scattered by the aluminium flakes. They were also obtained from analysis of successive photographs of the meridian cross-section. The frequency f_2' in the rotating frame was obtained from analysing successive photographs of the whole spherical surface in the laboratory at a particular reduced Reynolds number, $R^* = Re/Re_c = 2.2$, and also from the relationship among f_1, f_2 and f_2' which is discussed in

§5, using the measured values of f_1 and f_2.The amplitude, wavelength and azimuthal phase of the unmodulated and modulated waves were obtained by analysing timed photographs of the meridian cross-section in the laboratory frame.

The frequency scale used in the present study is expressed in units of the inner-sphere rotation frequency $\hat{f}_0$. Primed variables and the corresponding unprimed variables refer to the rotating and laboratory frames, respectively. The spectral resolution Δf, defined as $2f_N/N_d$, is about 0.005–0.01 for the Nyquist frequency $f_N = 10$–20 and the number of time-series records of scattered-light intensity, $N_d = 2048$ or 4097.

We obtained the required wavy and modulated wavy vortex flows by increasing the Reynolds number from zero to a particular value with a specific acceleration rate, as described later.

3. Experimental results and modal analysis of unmodulated waves

The schematic representation of the sources and sinks labelled j = a2–a2s and i2–i2s on the outer and inner spheres at the meridian cross-section of the spherical annulus, respectively, is illustrated in figure 2 for the toroidal TG vortex flow regime IIT with four vortex cells ($N = 4$). The labels and the characteristics of the flow regimes appearing in the present experiment are summarized in table 1. Although the modulated wavy vortex flow regime labelled IIIMWT, which will be described in §4, was found for the first time in the present experiment, the other flow regimes are the same as those reported earlier by Nakabayashi (1983). The unmodulated travelling azimuthal waves appearing on the toroidal TG vortices correspond to the singly periodic oscillations in meridian angles (colatitudes) θ_j of the sources and sinks j.

The complete wavy-vortex pattern consisting of four overlapping images of the spherical surface is shown in figure 3, for the case in which five azimuthal waves ($m = 5$) formed on the four toroidal cells ($N = 4$). These photos were taken using a mirror arrangement, as seen in Nakabayashi & Tsuchida (1988). The variable φ is the azimuthal angle, which is measured with respect to a reference frame fixed in the laboratory; it increases in the direction of sphere rotation. Following Coles (1965), the flow state of the wavy vortex flow is characterised by two integers, N and m, or N/m. Figure 3 shows the 4/5 state. The flow states with 2/4 and 4/6 can also be obtained by a particular mode of given R^* and $\dot{R}^*$ ($= \mathrm{d}R^*/\mathrm{d}T$, time T is expressed non-dimensionally in units of a characteristic time $R_1(R_2-R_1)/\nu$) for the present clearance ratio.

The flow state 4/5 is considered in the present study. The procedure for obtaining it is as follows. The inner sphere was rotated from rest and accelerated at a given rate ($\dot{R}^* \gtrsim 10^{-0.6}$) to a particular Reynolds number R_S^* ($R_S^* \gtrsim 2.8$), where a wavy vortex flow state with 4/6 (IIIWT) formed, as shown in figure 9. Then, R^* was quasi-statically increased to about 4.4, where the flow state changed from 4/6 to 4/5. The wavy vortex flow state with 4/5 can be continued in the range $2.5 \lesssim R^* \lesssim 7.2$, when R^* is quasi-statically varied.

The temporal oscillations in the meridian angles $\theta_j(t,\varphi)$ of the sources and sinks j, which are noted from analysis of the photographs of the meridian cross-section taken at fixed intervals over time at an azimuthal angle φ, are obtained for the $N/m = 4/5$ state, as indicated by the points in figure 4. The scale of the time t is expressed in units of the inner-sphere rotation period $1/\hat{f}_0$. Solid and broken lines represent least-square fits of the data to the sine functions given in (5). Although the data for j = a1 and a1s (omitted in the figure) barely show any oscillation, those for other j show

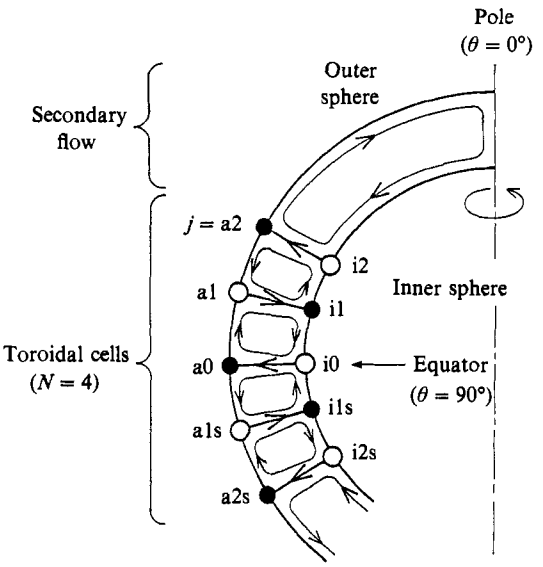

FIGURE 2. Schematic representation of streamlines, sources and sinks labelled j = a2–a2s and i2–i2s on the outer and inner spheres at the meridian cross-section, respectively, for the toroidal vortex flow state with four cells ($N = 4$); ○, source; ●, sink.

Flow regime	Characteristics
I B	Laminar flow + secondary flow (laminar basic flow)
II T	Laminar flow + toroidal TG vortex + secondary flow
II TS	Laminar flow + toroidal and spiral TG vortices + secondary flow
III WTS	Laminar flow + wavy toroidal and spiral TG vortices + secondary flow
III WT	Laminar flow + wavy toroidal TG vortex + secondary flow
III MWT	Laminar flow + modulated wavy toroidal TG vortex + secondary flow

TABLE 1. Flow regimes and their characteristics.

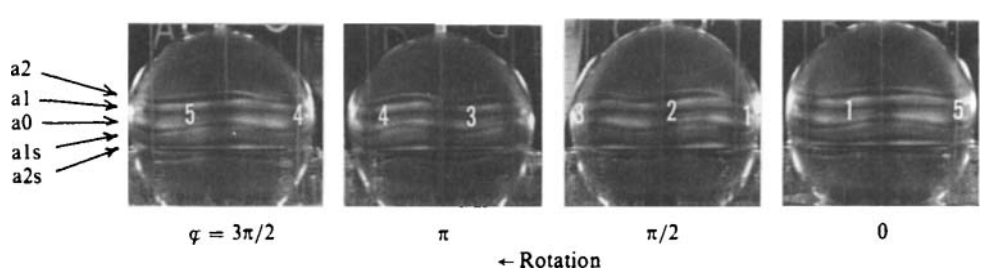

FIGURE 3. Complete wavy-vortex pattern for wavy-vortex-flow state with four toroidal cells and five azimuthal waves ($N/m = 4/5$) at $R^* = 4.33$ (photographed using a mirror arrangement). φ is the azimuthal angle, which is measured with respect to the laboratory and increases in the direction of sphere rotation. Successive waves around the annulus in the direction of wave rotation are labelled $1, 2, \ldots, m$.

entirely sinusoidal oscillations with the same frequency f_1, but each with a different amplitude A_j and temporal phase difference Δt_j from a reference time. Hence, both vortex inflow and outflow boundaries oscillate in SCF as well as CCF (Gorman & Swinney 1982), but the vortex inflow boundaries on the outer sphere are stationary for SCF. The time m/f_1 for m waves to pass an observer in the laboratory corresponds

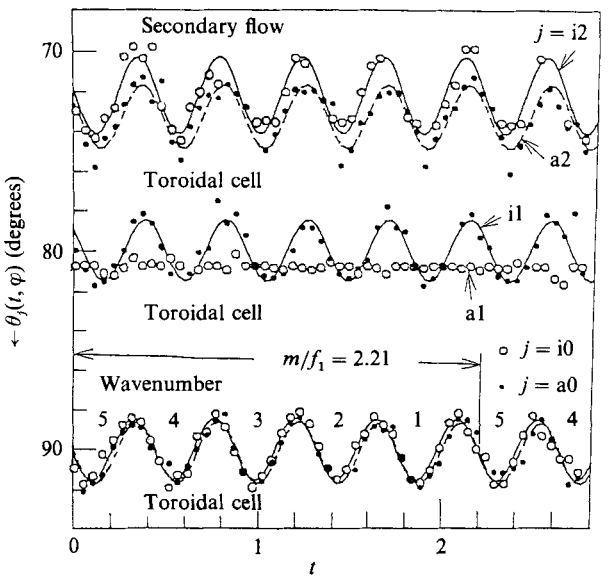

FIGURE 4. Temporal dependence of the meridian angles $\theta_j(t,\varphi)$ of the sources and sinks j at an azimuthal angle φ in the laboratory for the wavy-vortex-flow state with four toroidal cells and five azimuthal waves ($N/m = 4/5$) at $R^* = 5.19$. Experimental data: ○, source; ●, sink. The solid and broken lines represent least-square fits of the experimental data, on the inner and outer spheres respectively, to the sine functions given in (5). Successive waves in the negative time direction, corresponding to the direction of wave rotation, are labelled $1, 2, \ldots, m$.

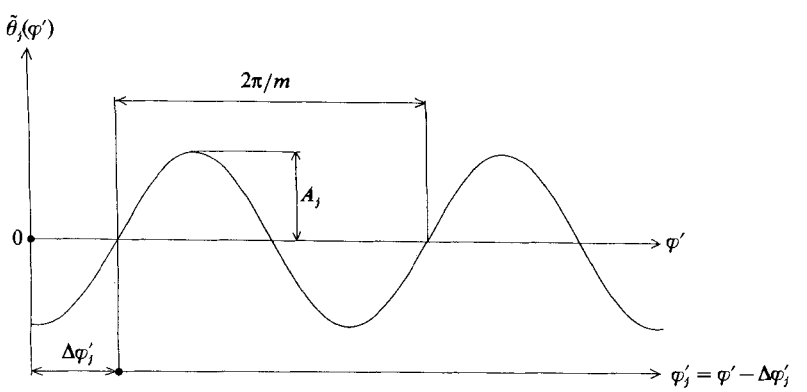

FIGURE 5. Schematic representation of the fluctuating colatitude,

$$\tilde{\theta}_j(\varphi') = A_j W(\varphi'_j) = A_j W(\varphi' - \Delta\varphi'_j),$$

of the source or sink j in the frame rotating with the travelling azimuthal waves. φ, φ'_j and $\Delta\varphi'_j$ ($= \varphi' - \varphi'_j$) are the reference azimuthal angle, the azimuthal angle for each j and the azimuthal phase difference between φ' and φ'_j, respectively. $W(\varphi'_j)$ describes the wave pattern in the rotating frame. A_j and $2\pi/m$ are the constant amplitude and the azimuthal wavelength, respectively.

to the rotation period of the travelling azimuthal waves. Since the rotation period m/f_1 is found to be 2.21 at $R^* = 5.19$ from figure 4, the rotation frequency f_1/m becomes 0.452. Thus, the wave pattern has m-fold rotational symmetry and rotates as a rigid body with rotation frequency f_1/m about the sphere axis; hence the pattern is at rest for an observer fixed in a reference frame rotating with the waves.

j	i0 Source	a0 Sink	i1 Sink	i2 Source	a2 Sink
Δt_j	0	0.0177	0.0546	0.0116	0.0372
$\Delta\varphi_j$	0°	−2.99°	−9.24°	−1.97°	−6.30°
$\Delta\varphi_j/\varphi_\lambda$	0	−0.0415	−0.128	−0.0274	−0.0874

TABLE 2. Temporal and azimuthal phase differences between the source i0 and other sources or sinks j, Δt_j and $\Delta\varphi_j$, and the ratio $\Delta\varphi_j/\varphi_\lambda$ for the wavy-vortex-flow state with four toroidal cells and five azimuthal waves ($N/m = 4/5$) at $R^* = 5.19$. Δt_j, $\Delta\varphi_j$ and $\varphi_\lambda = 2\pi/m$ are the temporal phase difference, the azimuthal phase difference and the azimuthal wavelength of the travelling azimuthal waves, respectively.

The fluctuating meridian angle, $\tilde{\theta}_j(\varphi') = \bar{\theta}_j - \theta_j(\varphi')$, for each j except for a1 and a1s in the rotating frame, is schematically illustrated in figure 5, where $\bar{\theta}_j$ is the average meridian angle, and φ' and φ'_j are the reference azimuthal angle and the azimuthal angle for each j, respectively. φ' and φ'_j are measured with respect to the rotating frame and increase in the direction of the sphere rotation; and $\Delta\varphi'_j = \varphi' - \varphi'_j$ is the azimuthal phase difference between φ' and φ'_j. For the modal analysis of the unmodulated travelling azimuthal waves, let the fluctuating meridian angle $\tilde{\theta}_j(\varphi')$ be assumed to take the form

$$\tilde{\theta}_j(\varphi') = \bar{\theta}_j - \theta_j(\varphi') = A_j W(\varphi'_j) = A_j W(\varphi' - \Delta\varphi'_j), \tag{1}$$

where A_j is the constant amplitude, and $W(\varphi'_j)$ describes the wave pattern and obeys

$$W\left(\varphi'_j + \frac{2\pi}{m}\right) = W(\varphi'_j).$$

Since the rotating frame rotates with angular speed $2\pi f_1/m$ with respect to the laboratory, φ and φ' are related by

$$\varphi' = \varphi - \frac{2\pi f_1 t}{m}. \tag{2}$$

The fluctuating meridian angle $\tilde{\theta}_j(t,\varphi)$ measured in the laboratory will then be

$$\begin{aligned}\tilde{\theta}_j(t,\varphi)\,\bar{\theta}_j - \theta_j(t,\varphi) &= A_j W\left(\varphi_j - \frac{2\pi f_1 t}{m}\right) \\ &= A_j W\left(\varphi - \frac{2\pi f_1 t}{m} - \Delta\varphi_j\right) \\ &= A_j W\left(\varphi - \frac{2\pi f_1 (t - \Delta t_j)}{m}\right),\end{aligned} \tag{3}$$

where $\Delta\varphi_j = \varphi - \varphi_j$ is the azimuthal phase difference between the reference azimuthal angle φ and the azimuthal angle φ_j for each j. $\Delta\varphi_j$ is equal to $\Delta\varphi'_j\,(= \varphi' - \varphi'_j)$, and Δt_j is the temporal phase difference related to the azimuthal phase difference $\Delta\varphi_j$ by

$$\Delta\varphi_j = -2\pi f_1 \Delta t_j. \tag{4}$$

If we assume $$W(\varphi'_j) = \sin(m\varphi'_j),$$

then (1) and (3) are written as

$$\tilde{\theta}_j(\varphi') = A_j \sin[m(\varphi' - \Delta\varphi'_j)]$$

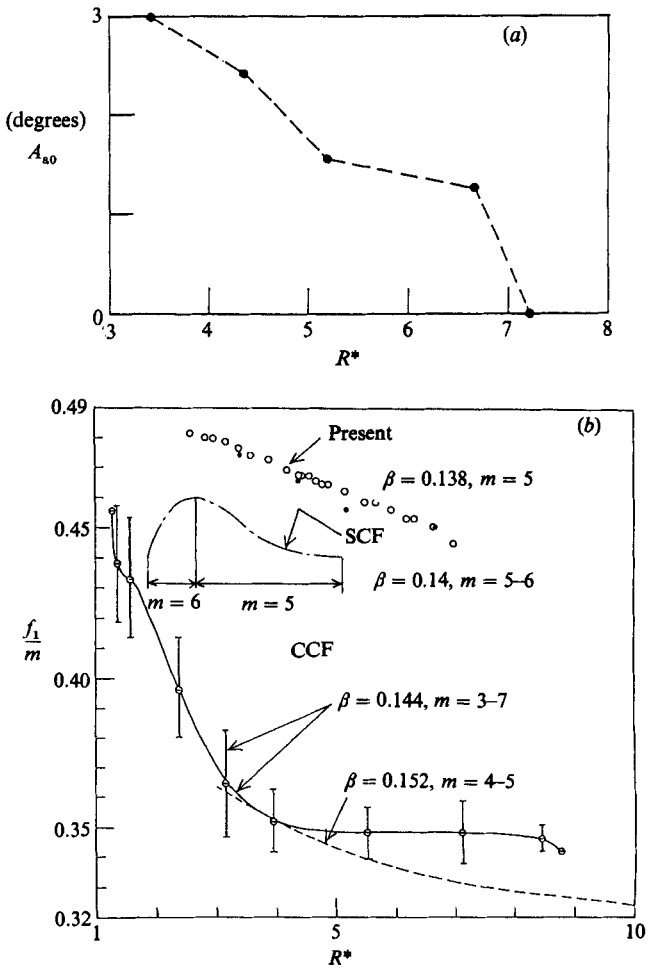

FIGURE 6. Reynolds-number dependence of the amplitude and the rotation frequency of the travelling azimuthal waves for the wavy-vortex-flow state with four toroidal cells and five azimuthal waves ($N/m = 4/5$). (*a*) Reynolds-number dependence of the amplitude A_{a0}. ● indicates the experimental data. (*b*) Reynolds-number dependence of the rotation frequency f_1/m. ○, ●, indicate the present data, obtained from the scattered-light-intensity power spectra and from the data in figure 4, respectively. The dashed–dotted line indicates data for the wavy-toroidal and spiral-TG-vortex-flow state with two toroidal cells, five or six azimuthal waves and one, two or three pairs of spiral TG vortices ($N = 2, m = 5$–$6, S_P = 1$–3) for $\beta = 0.14$, obtained by Nakabayashi & Tsuchida (1988) in spherical Couette flow. ⊖, the error bar Ϙ and the solid line show data for the wavy-vortex-flow state with $N = 18$–32 and $m = 3$–7 obtained by Coles (1965), in circular Couette flow with $\beta = 0.144, \Gamma = 27.9$. The broken line shows data for the wavy-vortex-flow state with $N = 0.833\Gamma$ and $m = 4$–5 obtained by King *et al.* (1984) for circular Couette flow with $\beta = 0.152, \Gamma_{max} = 80$.

and
$$\tilde{\theta}_j(t,\varphi) = \bar{\theta}_j - \theta_j(t,\varphi) = A_j \sin\left[m\left(\varphi - \frac{2\pi f_1(t-\Delta t_j)}{m}\right)\right], \tag{5}$$

respectively.

The values of Δt_j, $\Delta\varphi_j$, and the ratio of $\Delta\varphi_j$ to the azimuthal wavelength $\varphi_\lambda = 2\pi/m$ are given for each j at $R^* = 5.19$ in table 2, where the temporal and azimuthal phases for $j = \mathrm{i}0$ are chosen as reference phases ($\Delta t_{\mathrm{i}0} = \Delta\varphi_{\mathrm{i}0} = 0$). The temporal phase difference Δt_j is obtained from the sine function illustrated in figure 4, then $\Delta\varphi_j$ is calculated using (4). The temporal and azimuthal phases for $j = \mathrm{i}0$ are ahead of those

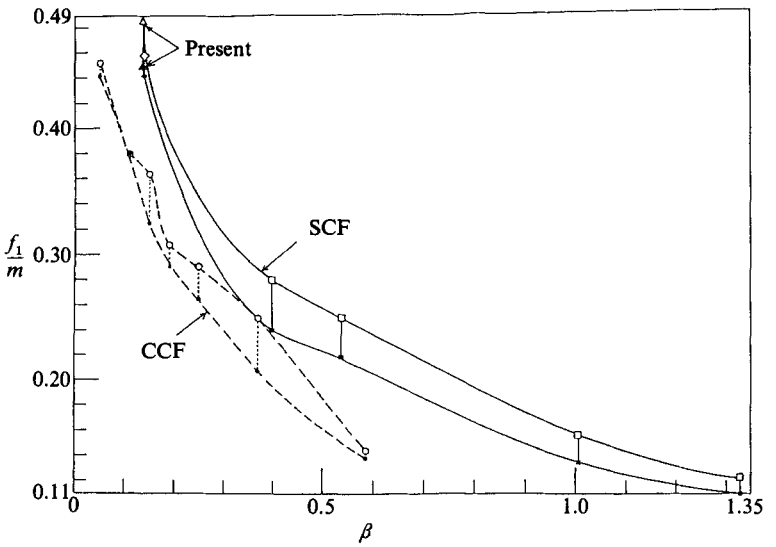

FIGURE 7. Clearance-ratio dependence of the rotation frequency of the travelling azimuthal waves. Spherical Couette flow: △, ▲, present data; ◇, ◆, Nakabayashi & Tsuchida (1988) ($\beta = 0.14$); □, ■, Yavorskaya *et al.* (1980) ($0.398 \leqq \beta \leqq 1.33$). Circular Couette flow: ○, ●, King *et al.* (1984) ($0.0526 \leqq \beta \leqq 0.588$). The open symbols show the maximum values, and the filled symbols the minimum values in the relationship between f_1/m and R^*.

for any other j. At $R^* = 5.19$, the difference of phases among all j is not great (less than $0.128\varphi_\lambda$, i.e. 0.128 waves), as indicated in the table. This difference is not great at other R^* either. Accordingly, all the waves in the meridian direction are considered to be in phase.

Now the amplitude and the rotation frequency f_1/m of the travelling azimuthal waves will be discussed. In figure 6(*a*) the relation between the amplitude for $j = \mathrm{a}0$, $A_{\mathrm{a}0}$, and R^* is shown. $A_{\mathrm{a}0}$ decreases with increasing R^* and becomes zero at $R^* \approx 7.2$, where the azimuthal waves disappear. The amplitude for any other j shows the same tendency as for $j = \mathrm{a}0$. In figure 6(*b*), the present data for f_1/m in the wavy-vortex-flow state with $m = 5$ decrease with increasing R^*, whereas the previous data (Nakabayashi & Tsuchida 1988) for f_1/m in the wavy toroidal and spiral TG vortex flow (flow regime III WTS) with $m = 5$ or 6 for $\beta = 0.14$ increase with R^* for $m = 6$, and decrease for $m = 5$. Thus, the rotation frequencies of the azimuthal waves in different flow regimes, III WT and III WTS, show the same tendency as R^* is increased if their wavenumbers are the same.

On the other hand, in CCF for $\beta = 0.144$ (Coles 1965, with aspect ratio $\Gamma = 27.9$), the wavy-vortex-flow states form with $m = 3$–7, and f_1/m decreases with increasing R^*, as shown in figure 6(*b*). For $\beta = 0.152$ (King *et al.* 1984, with maximum aspect ratio $\Gamma_{\max} = 80$), the wavy-vortex-flow states form with $m = 4$–5, and f_1/m decreases with R^*. The comparison of f_1/m from the present study with that from CCF shows that the former is greater than the latter, although the former displays the same tendency as the latter as R^* is increased.

The clearance-ratio dependence of the rotation frequency f_1/m is shown in figure 7, compared with that in CCF, where the range of uncertainty is obtained from the maximum and minimum values in the relationship between f_1/m and R^*, as shown in figure 6(*b*). Although the experimental results for $\beta = 0.138$, 0.14 in SCF, and for all β in CCF are for the travelling azimuthal waves appearing on the toroidal vortices,

the data for $\beta \geqq 0.398$ (Yavorskaya *et al.* 1980) in SCF are presumed to be for some velocity fluctuations appearing within the Ekman boundary layer, because no TG vortices occur for $\beta \geqq 0.398$. The rotation frequency for SCF has a similar clearance-ratio dependence to that for CCF, but the former is greater than the latter.

4. Experimental results for modulated waves

4.1. *The condition for the appearance of modulated waves*

In order to find the condition for the appearance of modulated travelling azimuthal waves (modulated wavy vortex flow), the flow is observed under the condition that R^* is increased from zero to R_S^* with an acceleration rate $\dot{R}^*$ and then is kept constant at R_S^*, as shown in figure 8. T is time, T_S is the time required for the acceleration, and T_h $(= T - T_S)$ is the time lapse after the acceleration has finished. All of these quantities are expressed non-dimensionally in units of a characteristic time $R_1(R_2 - R_1)/\nu$ adopted by Wimmer (1976).

The flow regime is transient with the lapse of time T, but eventually reaches some final flow regime independent of T. The dependence of the final flow regime on $\dot{R}^*$ and R_S^* is shown in figure 9. The labels I B, II T, II TS, III WTS, III WT and III MWT show the flow regimes, the characteristics of which are shown in table 1. The label III MWT + III WT indicates the flow regime in which III MWT and III WT appear alternately at intervals of several minutes, as shown in figure 10, where $t = 10$ corresponds to 37.5 s. No flow regime such as III MWT + III WT has been reported for CCF. As can be seen in figure 9, spiral TG vortices appear for $\dot{R}^* \lesssim 10^{-0.6}$, and modulation of waves III MWT cannot occur. However, under the condition of $\dot{R}^* \gtrsim 10^{-0.6}$ and $1.7 \lesssim R_S^* \lesssim 2.8$, no spiral TG vortices appear and modulation of waves can be obtained.

As described above, flow is transient with over time. Figure 11 shows the transition sequences from IB to the final flow regimes with time lapse T, comparing the greater acceleration case ($\dot{R}^* \gtrsim 10^{-0.6}$) and the smaller acceleration case ($\dot{R}^* \lesssim 10^{-0.6}$). In view of the difference in the transition process between the two cases, it is inferred that the necessary condition for the appearance of III MWT is the prevention of spiral TG vortices. Because of the greater acceleration, the transition from II T ($N = 2$) to II T ($N = 4$) occurs, then the transition to III WT and to III MWT occurs easily. It should be noted that N/m is 4/6 when the modulation occurs.

From another experiment, we found that III MWT can also be obtained by the quasi-static increase of R^*, once II T ($N = 4$) has been produced by some acceleration rates. Table 3 shows the observable sequence of flow regimes obtained by that procedure. For SCF, the modulation occurs simultaneously with the travelling azimuthal waves. However, for CCF (Fenstermacher *et al.* 1979), when R^* increases quasi-statically, unmodulated travelling azimuthal waves primarily appear, followed by the modulation.

4.2. *Characteristics of modulated waves*

When the modulation of the travelling azimuthal waves appeared in the flow state with $N/m = 4/6$ at $R^* = 2.2$, both the meridian cross-section of the spherical annulus and the whole spherical surface were photographed at fixed intervals over time. Figure 12(*a*) shows temporal oscillations in the meridian angles $\theta_j(t, \varphi)$ of the sources and sinks j shown in figure 2. These data are obtained by analysing successive photographs in the laboratory of the meridian cross-section at an azimuthal angle φ. Both the sources and sinks j (except $j =$ a1 and a1s) oscillate from an S-shape to a flattened shape (modulate) at the period $1/f_2 = 7/f_1$. As indicated by Gorman &

Reduced transition Reynolds number	Flow regime	Flow state N	m	k
—	II T	4	0	—
1.77	III MWT	4	6	−1
2.64	III MWT	4	6	−1
	+ III WT	4	6	—
2.80	III WT	4	6	—

TABLE 3. Sequence of the flow regimes observed when R^* is quasi-statically increased from the toroidal-vortex-flow state with four cells ($N = 4$). The label III MWT + III WT shows that the modulated wavy-vortex flow (III MWT) and the wavy-vortex flow (III WT) appear alternately.

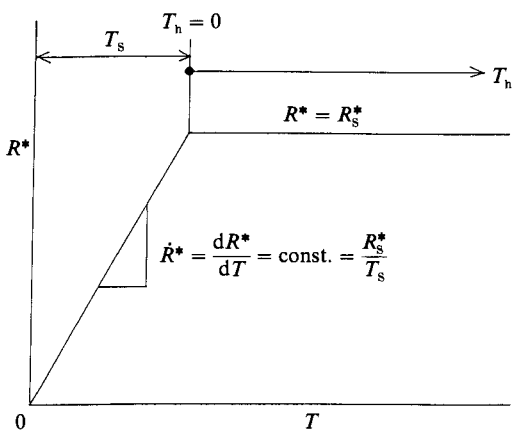

FIGURE 8. The condition for the time history of the reduced Reynolds number R^* adopted to examine the relationship between the appearance of the modulated wavy-vortex flow regime and the acceleration rate $\dot{R}^*$. R^* is $\dot{R}^*T$ for $0 \leqq T \leqq T_S$ and R_S^* for $T \geqq T_S$, where $\dot{R}^* = dR^*/dT = R_S^*/T_S$.

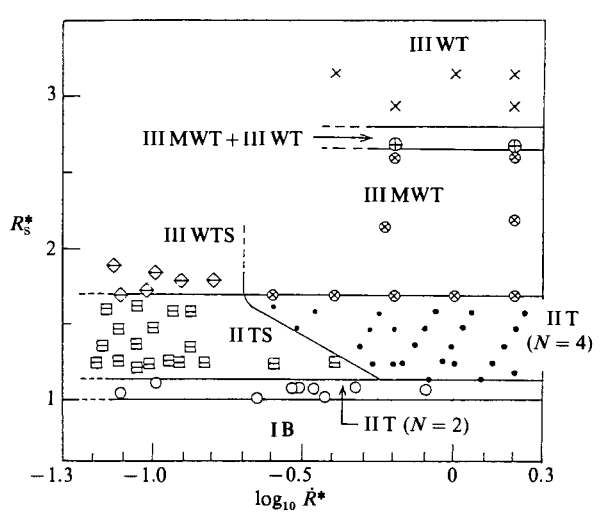

FIGURE 9. Dependence of the final flow regime on $\dot{R}^*$ and R_S^*. ×, III WT($N/m = 4/6$); ⊗, III MWT($N/m/k = 4/6/-1$); ⊕, III MWT($N/m/k = 4/6/-1$) + III WT($N/m = 4/6$); ●, II T($N = 4$); ○, II T($N = 2$); ⋄, III WTS($N = 2, m = 6, S_P = 3$–3), ⊟, II TS($N = 2, S_P = 3$–3). The variable S_P shows the number of pairs of spiral TG vortices in the northern ($0° < \theta < 90°$) and (–) southern ($90° < \theta < 180°$) hemispheres.

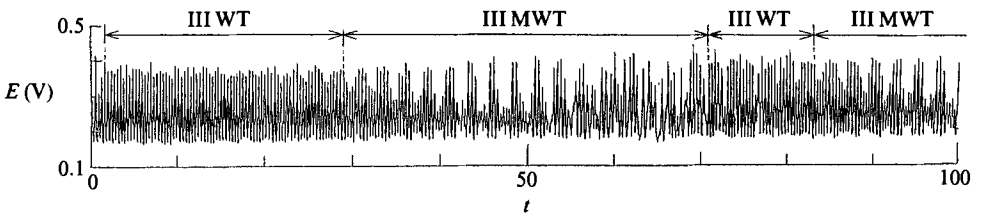

FIGURE 10. Temporal variation of the output E (V) of scattered-light intensity at $R^* = 2.64$ for the flow regime labelled III MWT + III WT, where the modulated wavy vortex flow (III MWT) and the wavy vortex flow (III WT) appear alternately.

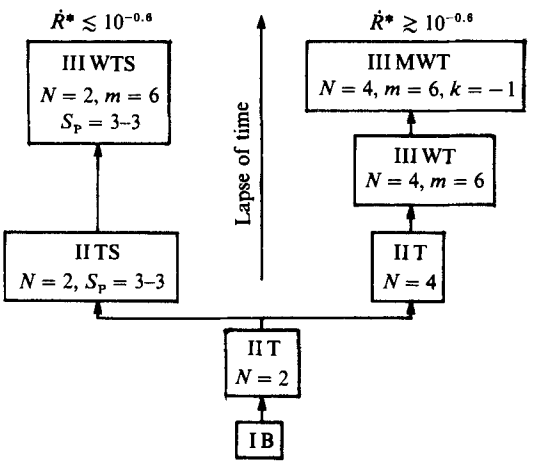

FIGURE 11. Sequence of transitions with the lapse of time T from laminar basic flow (IB) to wavy toroidal and spiral-TG-vortex flow (III WTS) for $\dot{R}^* \lesssim 10^{-0.6}$, or to modulated wavy-vortex flow (III MWT) for $\dot{R}^* \gtrsim 10^{-0.6}$, respectively.

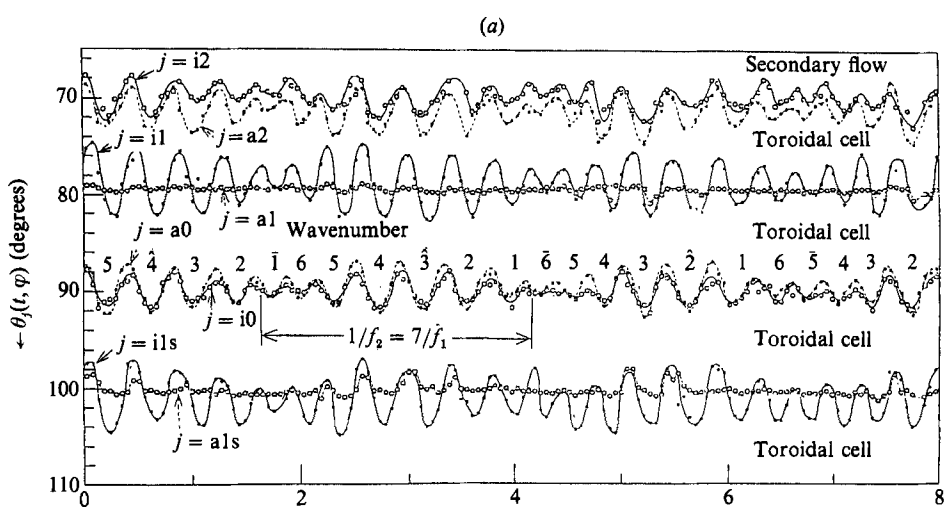

FIGURE 12(a). For caption see facing page.

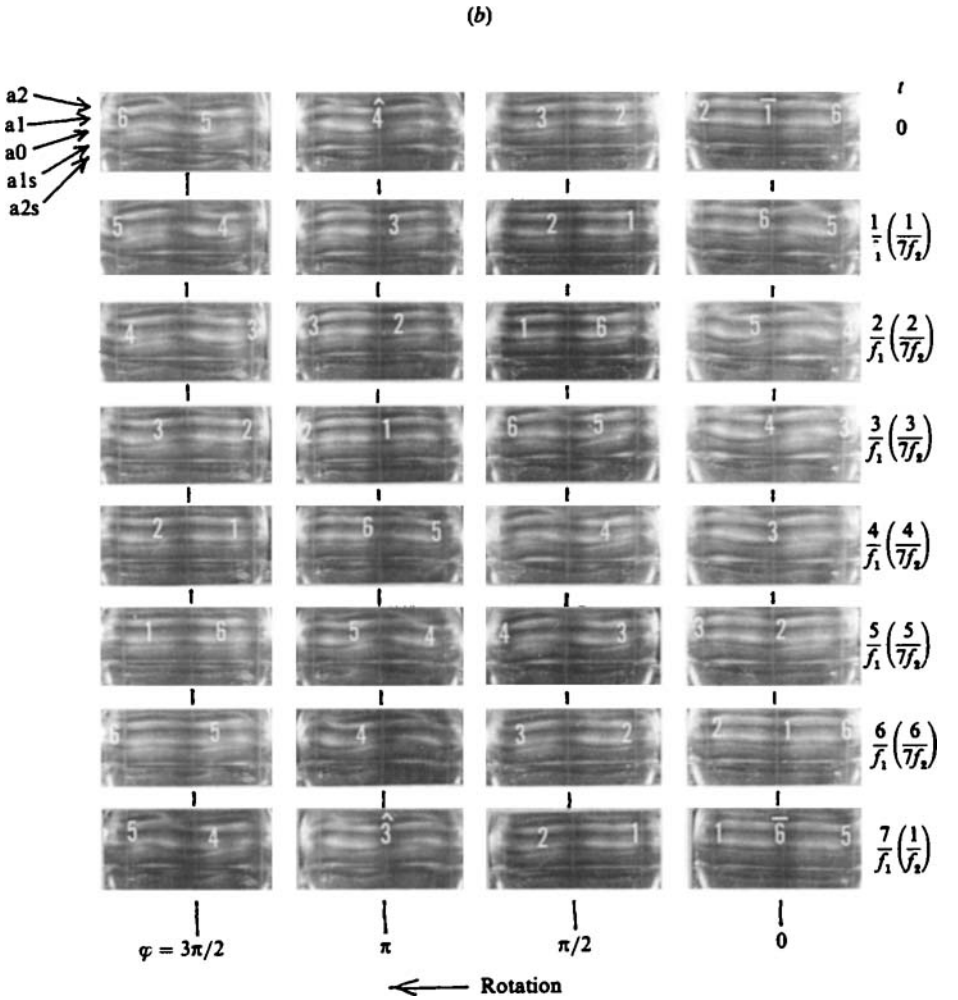

FIGURE 12. Temporal dependence of the meridan angles $\theta_j(t,\varphi)$ of the sources and sinks j at an azimuthal angle φ in the laboratory and photographs of the evolution in time of the modulation. Temporal dependence of the meridian angles and photographs of the evolution of the modulation pattern in the laboratory for the modulated wavy-vortex flow state with $N/m/k = 4/6/-1$ at $R^* = 2.2$. (*a*) Temporal dependence of the meridian angles $\theta_j(t,\varphi)$. ○ (source) and ● (sink) show the experimental data. Successive waves in the negative-time direction, corresponding to the direction of wave rotation, are labelled $1, 2, \ldots, m$. The waves with the bar and hat over the number are the flattened and S-shaped waves, respectively. $1/f_2$ is the modulation period in the laboratory. (*b*) Photographs of the evolution in time of the modulation pattern. Time t increases downward, and the azimuthal angle φ increases leftward. The time interval between the successive photographs is the average time $1/f_1$ for one wave to pass a point of observation in the laboratory. Waves are labelled as for (*a*).

Swinney (1982), a vortex outflow boundary periodically oscillates from an S-shape to a flattened shape in CCF. However, both vortex inflow and outflow boundaries similarly oscillate in the present study, even though the vortex inflow boundaries on the outer sphere are stationary, just as in the case of unmodulated waves (see figure 4). Figure 12(*b*) shows successive photographs of the whole spherical surface taken at the time interval, $1/f_1$, required for one wave to pass a point of observation in the

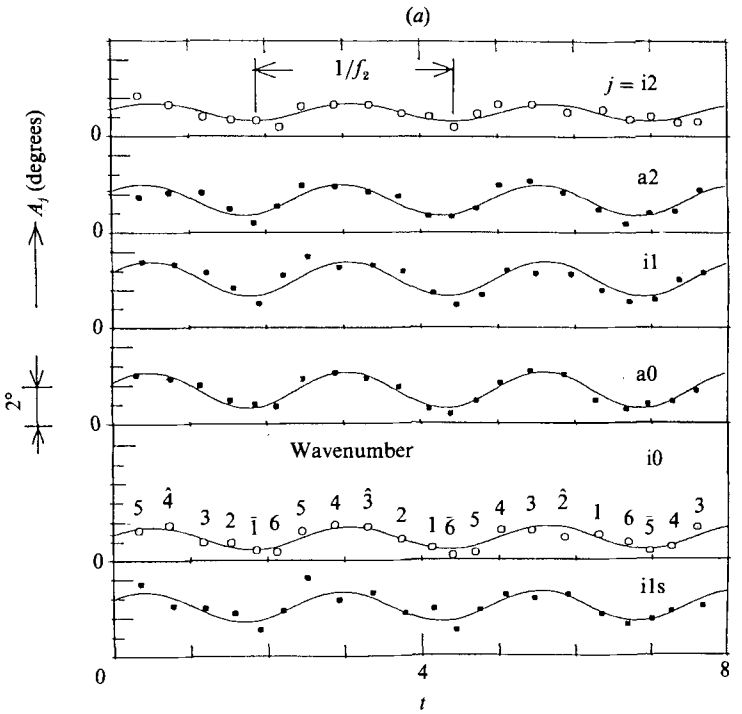

FIGURE 13(*a*). For caption see facing page.

laboratory, where time t increases downward, and the azimuthal angle φ in the laboratory increases leftward. The modulation pattern at $t = 0$ reappears at $t = 7/f_1$, which corresponds to $1/f_2 = 7/f_1$ in figure 12(*a*). From figure 12(*a*, *b*), the modulation frequency f_2 of the travelling azimuthal waves in the laboratory is given by

$$f_2 = \frac{f_1}{7} = 0.39 \quad (R^* = 2.2),$$

because $f_1 = 2.73$ at $R^* = 2.2$.

Amplitude A_j and temporal wavelength t_{Fj} of each individual wave were measured in figure 12(*a*), and plotted as a function of time at each individual wave node, as shown in figure 13(*a*, *b*). The flattened wave that has the smallest amplitude (greatest flattening) is indicated by the wavenumber with a bar over it (i.e. $\bar{1}$, $\bar{6}$ and $\bar{5}$). And the S-shaped wave with the greatest amplitude (most pronounced S-shaping) is indicated by a wavenumber with a hat over it (i.e. $\hat{4}$, $\hat{3}$ and $\hat{2}$). Solid lines in figure 13 represent least-square fits of the experimental data to sine functions given by

$$A_j = \bar{A}_j + \hat{A}_j \sin[2\pi f_{Aj}(t - \Delta t_{Aj})] \tag{6}$$

and

$$t_{Fj} = \bar{t}_{Fj} + \hat{t}_{Fj} \sin[2\pi f_{Fj}(t - \Delta t_{Fj})], \tag{7}$$

respectively, where $\bar{A}_j$ and $\bar{t}_{Fj}$ are average values, $\hat{A}_j$ and $\hat{t}_{Fj}$ are magnitudes of oscillation (modulation), f_{Aj} and f_{Fj} are modulation frequencies, and Δt_{Aj} and Δt_{Fj} are temporal phase differences from a reference time t. From figure 13(*a*), we found that

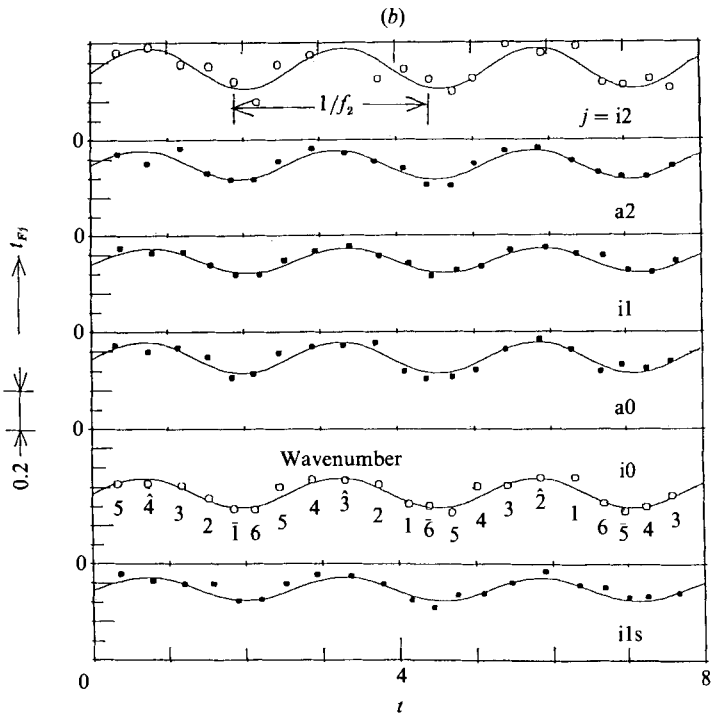

FIGURE 13. Amplitude and frequency modulations for the modulated wavy-vortex flow state with $N/m/k = 4/6/-1$ at $R^* = 2.2$. For description of wave labelling see figure 12. ○ (source) and ● (sink) are the experimental data. $1/f_2$ is the oscillation (modulation) period in the laboratory. (*a*) Temporal dependence of the amplitude of each individual modulated wave. The solid line represents the least-square fit of the experimental data to the sine function given by (6). (*b*) Temporal dependence of the temporal wavelength of each individual modulated wave. The solid line represents the least-square fit of the experimental data to the sine function given by (7).

the travelling azimuthal waves are amplitude modulated, and the period of amplitude modulation, $1/f_{Aj}$, is almost the same as $1/f_2$, i.e.

$$\frac{1}{f_A} = \frac{1}{f_2},$$

where j is omitted. Similarly, from figure 13(*b*) we found that the travelling azimuthal waves are frequency modulated, and that

$$\frac{1}{f_F} = \frac{1}{f_2}.$$

Hence, the travelling azimuthal waves are both amplitude and frequency modulated, and the frequencies of modulation are given by

$$f_A = f_F = f_2. \tag{8}$$

This equation is probably independent of R^* because the wave shape at other R^* values was visually confirmed to be almost the same as that at $R^* = 2.2$, as shown in figure 12.

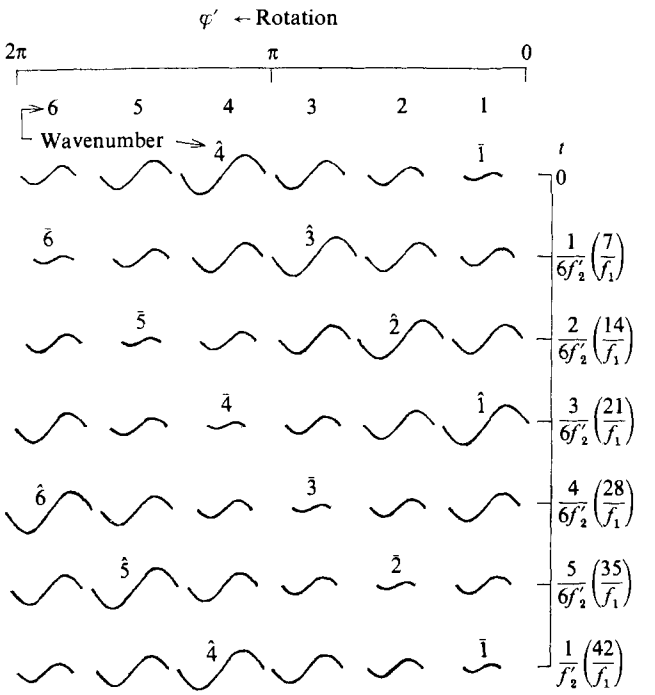

FIGURE 14. Schematic representation of the evolution in time of the modulation pattern in a reference frame rotating with the waves. Time t increases downward, and the azimuthal angle φ' in the rotating frame increases (from 0 to 2π) leftward. For description of wave labelling, see figure 12.

A schematic diagram showing the temporal evolution of modulation patterns in a reference frame rotating with the speed of the travelling azimuthal waves is shown in figure 14, where the time t increases downward, and the azimuthal angle φ' increases leftward. This diagram was obtained by analysing successive photographs of the whole spherical surface taken at the time interval $1/f_2 = 7/f_1$. Since the modulation pattern at $t = 0$ reappears at $t = 42/f_1$, the modulation frequency of both amplitude- and frequency-modulated travelling azimuthal waves in the rotating frame is given by

$$f_2' = \frac{f_1}{42} \quad (R^* = 2.2). \tag{9}$$

Hence, $f_2' = 0.065$ is obtained, because $f_1 = 2.73$ at $R^* = 2.2$.

From the relationship among the amplitude modulation, the frequency modulation and their superposed modulation in the laboratory given in (8), it is obvious that

$$f_A' = f_F' = f_2', \tag{10}$$

where f_A' and f_F' are the modulation frequencies of amplitude and frequency modulations, respectively, in the rotating frame.

In figure 14, the phase angle $\Delta\phi_A$ between the amplitude modulation of successive azimuthal waves is the same as the phase angle $\Delta\phi_F$ between the frequency modulation of successive azimuthal waves. Thus, the phase angle $\Delta\phi$ between the

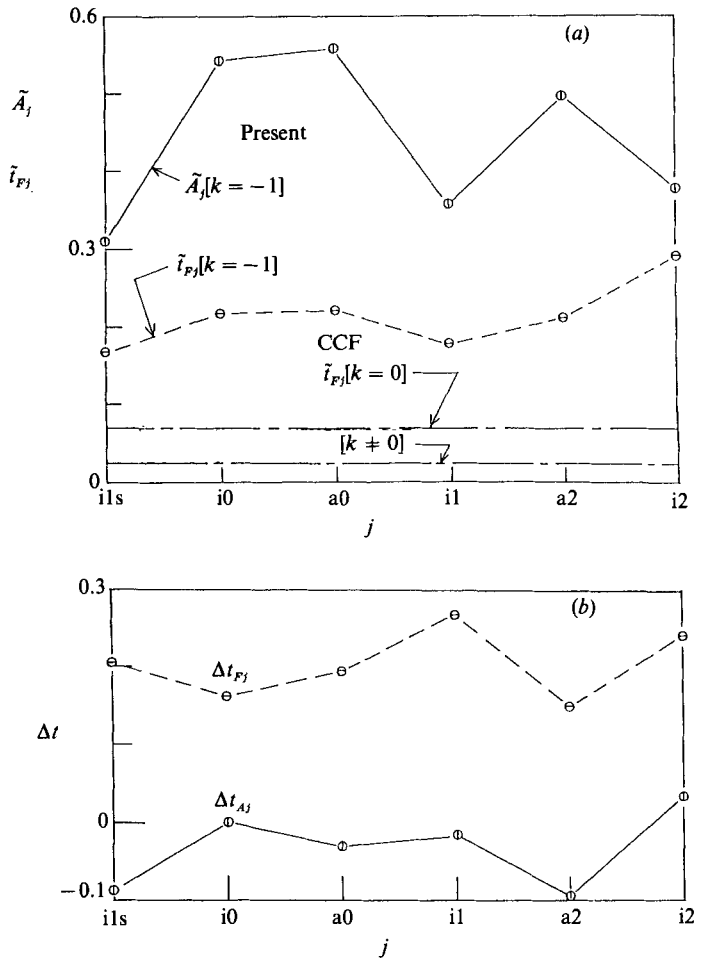

FIGURE 15. Magnitudes and temporal phase differences of the amplitude and frequency modulations for the modulated wavy-vortex-flow state with $N/m/k = 4/6/-1$ at $R^* = 2.2$. ⊕, ⊖, show the present data for the amplitude and frequency modulations, respectively. (*a*) Magnitudes, defined by $\tilde{A}_j = \hat{A}_j/\bar{A}_j$ and $\tilde{t}_{Fj} = \hat{t}_{Fj}/\bar{t}_{Fj}$, of the amplitude and frequency modulations, respectively, for each j. The dashed–dotted line shows the data obtained by Gorman & Swinney (1982) in circular Couette flow with $\beta = 0.133, \Gamma = 20$. (*b*) Temporal phase differences Δt_{Aj} and Δt_{Fj} of the amplitude and frequency modulations for each j. The phase for A_{i0} is chosen as a reference phase ($\Delta t_{Ai0} = 0$).

superposed modulation of the amplitude and frequency modulations of successive azimuthal waves is the same as $\Delta\phi_A$ and $\Delta\phi_F$, i.e.

$$\Delta\phi_A = \Delta\phi_F = \Delta\phi.$$

Since $\Delta\phi$ is independent of φ',

$$\Delta\phi = \frac{2\pi k}{m},$$

where k is a modulation parameter of the superposed modulation, just as for CCF (Swift *et al.* 1982). Similarly,

$$\Delta\phi_A = \frac{2\pi k_A}{m}, \quad \Delta\phi_F = \frac{2\pi k_F}{m},$$

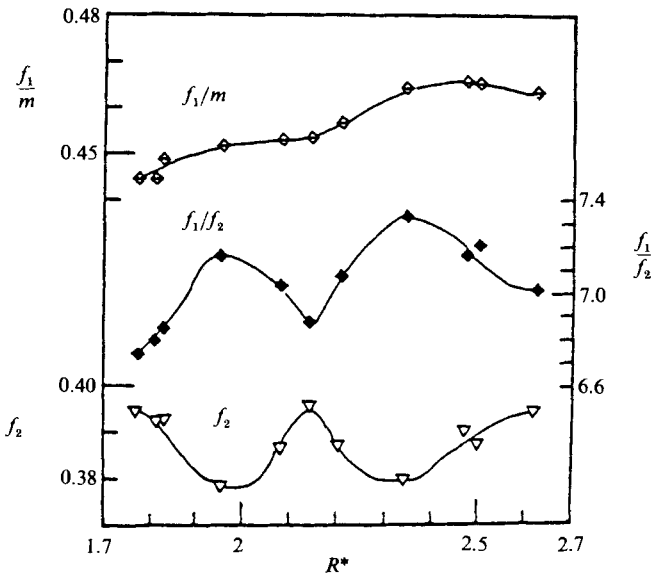

FIGURE 16. Reynolds-number dependence of the rotation frequency f_1/m of the modulated travelling azimuthal waves, the modulation frequency f_2 measured in the laboratory and the ratio of f_1/f_2 for the modulated wavy-vortex flow state with $N/m/k = 4/6/-1$. ⊖, ▽, ◆ indicate the experimental data for $f_1/m, f_2, f_1/f_2$, respectively.

where k_A and k_F are modulation parameters of the amplitude and frequency modulations, respectively. Consequently,

$$k_A = k_F = k. \tag{11}$$

The values of k_A, k_F and k are -1 in figure 14 (Gorman & Swinney 1982). This equation is probably independent of R^*, because the wave shape at other R^* values was confirmed to be almost the same as that at $R^* = 2.2$, as described previously.

Figure 15(*a*) shows the magnitudes defined by $\tilde{A}_j = \hat{A}_j/\bar{A}_j$ and $\tilde{t}_{Fj} = \hat{t}_{Fj}/\bar{t}_{Fj}$ for each j, which were calculated from the results in figure 13. Since $\tilde{A}_j > \tilde{t}_{Fj}$, the magnitude of amplitude modulation is greater than that of frequency modulation. On the other hand, for CCF Gorman & Swinney (1982) measured the time for successive waves to pass an observer in the laboratory by analysing ciné films frame by frame. They obtained the deviation from the mean time of arrival of waves for the modulated wavy-vortex-flow states with $k = 0$ ($m = 4$ and 5) and $k \neq 0$. Their data are shown in figure 15 by dashed-and-dotted lines, where the difference in $\tilde{t}_{Fj}$ by j (vortex outflow boundary) is neglected because it was not reported. The magnitude of frequency modulation in SCF is much greater than that in CCF. The temporal phase differences Δt_{Aj} and Δt_{Fj}, which were calculated from the results in figure 13, are indicated for each j in figure 15(*b*), where the phase of A_{i0} shown in figure 13(*a*) is a reference phase ($\Delta t_{Ai0} = 0$). For an observer in the laboratory the phase of the amplitude modulation is slightly ahead of that of the frequency modulation, because $\Delta t_F \approx \Delta t_A + 0.1/f_2$ ($0.1/f_2 = 0.7/f_1 = 0.25$) for all j, where j is omitted. $\Delta t_F = \Delta t_A$ means that the S-shaped wave has the greatest wavelength and the flattened wave has the smallest wavelength, while $\Delta t_F = \Delta t_A \pm 0.5/f_2$ means that the former has the smallest wavelength and the latter has the greatest wavelength, as can be seen in (6) and (7). Accordingly, the former is elongated and the latter is shortened in

	Present	CCF
β	0.138	0.133
Γ	—	20
m	6	6
k	−1	−1
N	4	20
R^*	1.77 ~ 2.64	10.5 (onset)
f_1	2.730±0.066	2.03
f_1/m	0.455±0.011	0.34
f_2	0.387±0.009	0.21
f_2'	0.066±0.018	0.55
Relation	$f_2' = -f_2 - kf_1/m$	$f_2' = f_2 - kf_1/m$

TABLE 4. Comparison of characteristics of the modulated wavy-vortex-flow state with $m = 6$ and $k = -1$ for the present data with those for circular Couette flow (Gorman & Swinney 1982). The relationships among the characteristic frequencies are described in §5. The values of characteristic frequencies in circular Couette flow are obtained at its observed onset ($R^* = 10.5$).

the present results, whereas the former is shortened and the latter is elongated ($\Delta t_F \approx \Delta t_A \pm 0.5/f_2$) in CCF (Gorman & Swinney 1982).

The Reynolds-number dependence of the rotation frequency f_1/m, the modulation frequency f_2 and the ratio, f_1/f_2, is shown in figure 16 for the modulated wavy-vortex-flow state with $N/m/k = 4/6/-1$. The values of f_1/m and f_1/f_2 were calculated from the measured values of f_1, f_2 and m. The values of f_1 and f_2 that were determined from the power spectra of the intensity of laser light reflected by the aluminium flakes suspended in the fluid agree with those determined by visual observation using a stop-watch. Both the absolute and relative amplitudes of the components of the power spectra varied considerably, depending on the position of the laser beam in the annulus, but the components of the frequencies were independent of the scattering position. The value of m was determined by flow visualization, as described in §2. The f_1/m value tends to increase with R^*. This tendency is similar to the dependence of f_1/m on R^* for the wavy toroidal and spiral TG vortex flow state with $m = 6$ in figure 6(*b*). However, if the f_1/m value is considered to be approximately constant, it is given by

$$f_1/m = 0.455 \pm 0.011\ (\pm 2.4\,\%).$$

The variation ± 0.011 is greater than the spectral resolution $\Delta f/m = 0.0008$–0.0016, so that the f_1/m value is probably dependent on R^*. On the other hand, the f_2 value is given by

$$f_2 = 0.387 \pm 0.009\ (\pm 2.3\,\%).$$

The variation ± 0.009 is on the same order as the spectral resolution $\Delta f = 0.005$–0.01. The f_1/f_2 value varies with increasing R^*, as shown in figure 16, and is given by

$$f_1/f_2 = 7.03 \pm 0.30\ (\pm 4.3\,\%). \tag{12}$$

And the relatively large variation ± 0.30 does not seem to corroborate the frequency entrainment (i.e. over some range of R^*, f_1/f_2 is not given by the ratio of small integers).

For CCF (Gorman & Swinney 1982), f_1 in the doubly periodic flow regime is independent of R^* within the 1 % experimental uncertainty; however, the variation of f_1 (for a given m) as a function of k is as much as 3 %, greater than the experimental

uncertainty and $f_1/m = 0.34 \pm 0.01$ ($\pm 2.9\%$) for all R^*, N, m and k. On the other hand, f_1/m for SCF depends on R^*, as described above, and is greater than that for CCF, just as for unmodulated waves (see §3). The f_2 value for CCF increases monotonically with increasing R^* and the total increase over the whole modulated wavy-vortex-flow region is at most 20%, whereas f_2 for SCF is virtually independent of R^*, as described above. The ratio f_1/f_2 for CCF is a strictly decreasing smooth function of R^* for all flow states, whereas f_1/f_2 for SCF has a tendency to increase with R^*, as shown in figure 16. Thus, f_1/f_2 probably depends on R^* for SCF as well as CCF, so that the absence of frequency entrainment is corroborated for SCF as well as CCF.

The characteristics of the modulated wavy-vortex-flow state obtained in the present study are summarized in table 4, and compared with those of the modulated wavy-vortex-flow state with $m = 6$ and $k = -1$ in CCF. Rand (1981) used dynamic-systems concepts and symmetry considerations to derive predictions about the space–time symmetry of doubly periodic flows in circularly symmetric systems. He predicted that only flows with certain space–time symmetries should be allowed. Gorman & Swinney (1982) discovered twelve doubly periodic flow (m, k) states in CCF, indicating that the observed flow states are in agreement with Rand's theory. Although in SCF the unobserved modulated wavy-vortex-flow states might be stable, we have not yet found a way of producing them. The modulated wavy-vortex-flow state for SCF is located in a much lower R^* range than for CCF.

5. Modal analysis of modulated waves

For a modal analysis of the modulated travelling azimuthal waves, the fluctuating values $\tilde{\theta}_j(t,\varphi')$ of the meridian angles $\theta_j(t,\varphi')$ of the sources and sinks j at time t and an azimuthal angle φ' in a reference frame that rotates in phase with the azimuthal waves can be assumed to take the form

$$\tilde{\theta}_j(t,\varphi') = \bar{\theta}_j - \theta_j(t,\varphi') = A_j(t,\varphi')\, W(t,\varphi'), \tag{13}$$

following Swift *et al.* (1982). $\bar{\theta}_j$ is the average of $\theta_j(t,\varphi')$, and $A_j(t,\varphi')$ and $W(t,\varphi')$ give the fluctuating amplitude (amplitude modulation) and the fluctuating wave pattern (frequency modulation), respectively. The reason why W describing the wave pattern is here assumed to be $W(t,\varphi')$ instead of the $W(\varphi')$ in the modal analysis of Swift *et al.* for CCF is that frequency modulation as well as amplitude modulation is included in the present study. Let f'_A and f'_F be the frequencies of amplitude and frequency modulations, respectively, in the rotating frame. Then $A_j(t,\varphi')$ and $W(t,\varphi')$ obey

$$A_j\left(t+\frac{1}{f'_A},\varphi'\right) = A_j(t,\varphi'), \quad W\left(t+\frac{1}{f'_F},\varphi'\right) = W(t,\varphi'), \tag{14}$$

respectively. Further, $A_j(t,\varphi')$ and $W(t,\varphi')$ obey

$$A_j(t,\varphi'+2\pi) = A_j(t,\varphi'), \quad W(t,\varphi'+2\pi) = W(t,\varphi'), \tag{15}$$

respectively, because they must be periodic functions with a period 2π. We introduce phase angles $\phi_A(\varphi')$ and $\phi_F(\varphi')$ for the amplitude and frequency modulations, respectively. Then we may write

$$A_j(t,\varphi') = a_j[2\pi f'_A t - \phi_A(\varphi')], \quad W(t,\varphi') = w[2\pi f'_F t - \phi_F(\varphi')], \tag{16}$$

where a_j and w are periodic functions of each argument with a period 2π, just as Swift

et al. (1982) introduced a phase angle for the amplitude modulation in CCF. For $A_j(t,\varphi')$ and $W(t,\varphi')$ in (16) to satisfy (15) we must have

$$\phi_D(\varphi'+2\pi)=\phi_D(\varphi')+2\pi k_D \quad (k_D\in Z), \tag{17}$$

where Z is a set of integers, and the subscript D is used instead of the subscripts A and F in order to shorten the description. As described in §4.2, the phase difference $\Delta\phi_D$ between the modulation of adjacent waves is the same; i.e.

$$\Delta\phi_D=\phi_D\left(\varphi'+\frac{2\pi}{m}\right)-\phi_D(\varphi')=\frac{2\pi k_D}{m}.$$

We can without loss of generality restrict the integer k_D to the range

$$-\tfrac{1}{2}m<k_D\leqq\tfrac{1}{2}m \quad (k_D\in Z),$$

since ϕ_D is modulo 2π. In this case, we may then write

$$\phi_D(\varphi')=\chi_D(\varphi')+k_D\varphi', \tag{18}$$

$$\chi_D\left(\varphi'+\frac{2\pi}{m}\right)=\chi_D(\varphi'). \tag{19}$$

Substitution of (16), (18) and (19) in (13) yields

$$\tilde{\theta}_j(t,\varphi')=a_j[2\pi f'_A t-\chi_A(\varphi')-k_A\varphi']\,w[2\pi f'_F t-\chi_F(\varphi')-k_F\varphi']. \tag{20}$$

Since the frequency f'_2 in the rotating frame is the modulation frequency of $\tilde{\theta}_j(t,\varphi')$, including both amplitude and frequency modulations, $\tilde{\theta}_j(t,\varphi')$ must obey

$$\tilde{\theta}_j\left(t+\frac{1}{f'_2},\varphi'\right)=\tilde{\theta}_j(t,\varphi'). \tag{21}$$

From (20), (21) and the periodicities of the periodic functions a_j and w, we obtain

$$f'_D=i'_{D2}f'_2 \quad (i'_{D2}\in Z). \tag{22}$$

The equation, which $\tilde{\theta}_j(t,\varphi')$ must also obey,

$$\theta_j(t,\varphi'+2\pi)=\theta_j(t,\varphi') \tag{23}$$

is easily confirmed from (19), (20) and the periodicities of the functions a_j and w. Substitution of (22) into (20) yields

$$\tilde{\theta}_j(t,\varphi')=a_j[2\pi i'_{A2}f'_2 t-\chi_A(\varphi')-k_A\varphi']\,w[2\pi i'_{F2}f'_2 t-\chi_F(\varphi')-k_F\varphi']. \tag{24}$$

From substitution of (2) in (24) the fluctuating value $\tilde{\theta}_j(t,\varphi)$ of the meridian angle $\theta_j(t,\varphi)$ at time t and an azimuthal angle φ in the laboratory will be obtained as

$$\begin{aligned}\tilde{\theta}_j(t,\varphi)&=\bar{\theta}_j-\theta_j(t,\varphi)\\&=a_j\left[2\pi\left(i'_{A2}f'_2+\frac{k_A f_1}{m}\right)t-\chi_A\left(\varphi-\frac{2\pi f_1 t}{m}\right)-k_A\varphi\right]\\&\quad\times w\left[2\pi\left(i'_{F2}f'_2+\frac{k_F f_1}{m}\right)t-\chi_F\left(\varphi-\frac{2\pi f_1 t}{m}\right)-k_F\varphi\right].\end{aligned} \tag{25}$$

Since the frequencies f_2, f_A, and f_F are the modulation frequencies of the superposed

modulation of amplitude and frequency modulations, the amplitude modulation and the frequency modulation, $\tilde{\theta}_j(t,\varphi)$, $A_j(t,\varphi)$ and $W(t,\varphi)$ obey, respectively,

$$\tilde{\theta}_j\left(t+\frac{1}{f_2},\varphi\right)=\tilde{\theta}_j(t,\varphi), \tag{26}$$

$$A_j\left(t+\frac{1}{f_A},\varphi\right)=A_j(t,\varphi), \quad W\left(t+\frac{1}{f_F},\varphi\right)=W(t,\varphi). \tag{27}$$

From (16), (19), (25), (26), (27) and the periodicities of the functions a_j and w, we obtain

$$f_2=\frac{i'_{D2}f'_2+k_Df_1/m}{i_{D2}} \quad (i_{D2}\in Z), \tag{28}$$

$$f_D=\frac{i'_{D2}f'_2+k_Df_1/m}{i_{DD}}=\frac{i_{D2}f_2}{i_{DD}} \quad (i_{DD}\in Z), \tag{29}$$

$$f_2=\frac{f_1}{i_{12}}, \tag{30}$$

$$f_D=\frac{f_1}{i_{1D}}=\frac{i_{12}f_2}{i_{1D}}. \tag{31}$$

When $\chi_D(\varphi')$ in (18) is a periodic function with a period $2\pi/m$, as (19) shows, the variables i_{12} in (30) and (31) and i_{1D} in (31) must be integers for this periodicity to be satisfied. But when $\chi_D(\varphi')$ is a constant, as a special case, i_{12} and i_{1D} need not be integers because the above periodicity becomes meaningless. Since i_{12} and i_{1D} are not always integers as R^* is varied, as we shall see later, $\chi_D(\varphi')$ seems to be a constant. The requirement that $\tilde{\theta}_j(t,\varphi)$, $A_j(t,\varphi)$ and $W(t,\varphi)$ must be periodic functions with period 2π is easily confirmed by (2), (15) and (23). Substitution of (28) in (25) yields

$$\tilde{\theta}_j(t,\varphi)=a_j\left[2\pi i_{A2}f_2t-\chi_A\left(\varphi-\frac{2\pi f_1t}{m}\right)-k_A\varphi\right]w\left[2\pi i_{F2}f_2t-\chi_F\left(\varphi-\frac{2\pi f_1t}{m}\right)-k_F\varphi\right].$$

The present results, (8), (10), (11), (12) and table 4, obtained in the range $1.77 \leqq R^* < 2.64$ for the modulated wavy vortex flow are summarized as

$$k_D=k, \tag{32}$$

$$f'_D=f'_2, \quad f_D=f_2, \tag{33}$$

$$f_1/f_2=7.03\pm0.30 \quad m=6, \quad k=-1. \tag{34}$$

Although the f'_2 value in the rotating frame was only measured from successive photographs, as described in §4.2, for $R^*=2.2$, it can be assumed to be approximately

$$f'_2=f_1/42 \text{ (assumption)}, \tag{35}$$

as shown in (9), because the wave shape at other R^* values was confirmed to be almost the same as that at $R^*=2.2$. Substitution of (32)–(35) in (22) and (28)–(31) yields

$$i'_{D2}=\frac{f'_D}{f'_2}=1, \tag{36}$$

$$i_{D2}=\left(i'_{D2}f'_2+\frac{k_Df_1}{m}\right)/f_2=\left(f'_2+\frac{kf_1}{m}\right)/f_2\approx\frac{(1/42+k/m)f_1}{f_2}=-1\pm0.004, \tag{37}$$

$$i_{DD} = \frac{i_{D2} f_2}{f_D} = i_{D2} \approx -1 \pm 0.004, \tag{38}$$

$$i_{12} = \frac{f_1}{f_2} = 7.03 \pm 0.30, \tag{39}$$

$$i_{1D} = \frac{i_{12} f_2}{f_D} = i_{12} = 7.03 \pm 0.30. \tag{40}$$

Since the variables i_{D2} in (37) and i_{DD} in (38) must be integers as shown in (28) and (29), respectively, they are presumed to be

$$i_{D2} = \frac{i'_{D2} f'_2 + k_D f_1/m}{f_2} = \frac{f'_2 + k f_1/m}{f_2} = -1 \tag{41}$$

and

$$i_{DD} = \frac{i_{D2} f_2}{f_D} = i_{D2} = -1,$$

respectively. Equation (41) is rewritten as

$$f'_2 = -f_2 - \frac{k f_1}{m}. \tag{42}$$

Since i_{12} and i_{1D} are not always integers from (39) and (40), $\chi_D(\varphi')$ in (18) seems to be a constant, not a periodic function with a period $2\pi/m$ as Swift *et al.* (1982) assumed in (19), as described previously.

Although the results of (32) and (36) are the same as those given by Gorman & Swinney (1982) for CCF, the results of (39) and (41) are different from those for CCF, where i_{12} and i_{D2} are given as

$$i_{12} = \frac{f_1}{f_2} = 9.67 \quad (m = 6, \quad k = -1, \quad R^* = 10.5 \text{ (onset)}, \quad \text{CCF}),$$

$$i_{D2} = \frac{i'_{D2} f'_2 + k_D f_1/m}{f_2} = \frac{f'_2 + k f_1/m}{f_2} = 1 \quad \text{(CCF)}.$$

Since the i_{12} value depends on R^* (which, of course, depends on N, m and k) for CCF, i_{12} is not always an integer, and consequently $\chi_D(\varphi')$ in (18) must be a constant for CCF as well as SCF. Nevertheless, Swift *et al.* (1982) simulated the $\chi_A(\varphi')$ for the amplitude modulation as

$$\chi_A(\varphi') = \text{int}\left[\frac{m\varphi'}{2\pi}\right] - k\varphi' \quad \text{(CCF)}$$

for the modulated wavy-vortex-flow state with $m = 4$ and $k = 1$ for CCF. Since Gorman & Swinney (1982) obtained the following result:

$$i_{12} = \frac{f_1}{f_2} = 1.68 \quad (m = 4, \quad k = 1, \quad R^* = 10.2 \text{ (onset)}, \quad \text{CCF}),$$

The above simulation is not reasonable with respect to putting $\chi_A(\varphi') \neq \text{const}$.

For a quantitative comparison with the experimental data, we have generated synthetic time-series files using the specific functions that were adopted by Ohji, Shionoya & Amagai (1986) for CCF, namely

$$\chi_D(\varphi') = c_{Dj}, \quad \phi_D(\varphi') = \chi_D(\varphi') + k_D\varphi' = c_{Dj} + k_D\varphi'$$

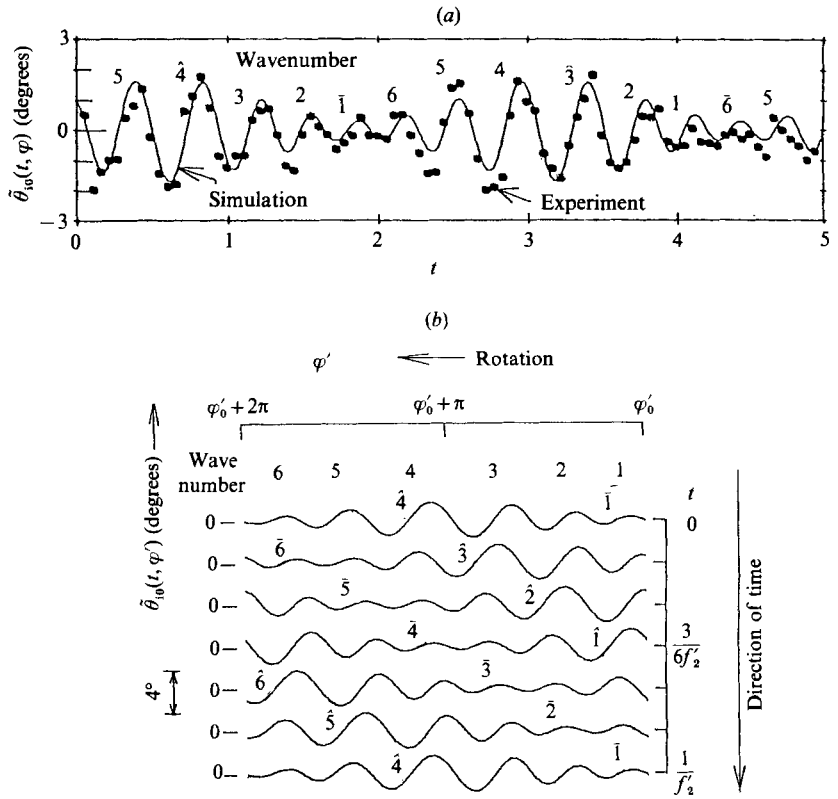

FIGURE 17. Simulation of modulated waves for modulated wavy-vortex flow state with $N/m/k = 4/6/-1$ at $R^* = 2.2$. For description of wave labelling see figure 12. (*a*) Temporal dependence of the fluctuating meridian angle $\tilde{\theta}_{i0}(t,\varphi)$ in the laboratory. ● indicates experimental data. The solid line is the simulation given by (45). (*b*) Azimuthal and temporal dependence of the fluctuating meridian angle $\tilde{\theta}_{i0}(t,\varphi')$ in the rotating frame simulated by (44). The φ'_0 value is 0.675π.

$$\left.\begin{aligned} &\text{and} \quad a_j[2\pi f'_A t - \phi_A(\varphi')] = \bar{a}_j + \hat{a}_j \sin(2\pi f'_A t - c_{Aj} - k_A\varphi'),\\ &\qquad w[2\pi f'_F t - \phi_F(\varphi')] = \sin[m\varphi' + \bar{w}_j + \hat{w}_j \sin(2\pi f'_F t - c_{Fj} - k_F\varphi')], \end{aligned}\right\} \tag{43}$$

where $\bar{a}_j, \hat{a}_j, c_{Aj}, \bar{w}_j, \hat{w}_j, c_{Fj}$ are constants. Although Ohji *et al.* (1986) assumed $\chi_D(\varphi') =$ constant without any discussion, the reason for this are as described above. Substitution of (22) and (43) in (24) yields

$$\begin{aligned} \tilde{\theta}_j(t,\varphi') = [\bar{a}_j + \hat{a}_j \sin(2\pi i'_{A2} f'_2 t - c_{Aj} - k_A\varphi')]\\ \times \sin[m\varphi' + \bar{w}_j + \hat{w}_j \sin(2\pi i'_{F2} f'_2 t - c_{Fj} - k_F\varphi')]. \end{aligned} \tag{44}$$

Further, substitution of (2) and (28) in (44) yields

$$\begin{aligned} \tilde{\theta}_j(t,\varphi) = [\bar{a}_j + \hat{a}_j \sin(2\pi i_{A2} f_2 t - c_{Aj} - k_A\varphi)]\\ \times \sin\left[m\left(\varphi - \frac{2\pi f_1 t}{m}\right) + \bar{w}_j + \hat{w}_j \sin(2\pi i_{F2} f_2 t - c_{Fj} - k_F\varphi)\right]. \end{aligned} \tag{45}$$

The temporal dependence of the fluctuating value $\theta_{i0}(t,\varphi)$ of the source i0 at an azimuthal angle φ in the laboratory is shown by the points in figure 17 (*a*), which is obtained from the experimental data of the meridian angle $\theta_{i0}(t,\varphi)$ at $R^* = 2.2$ in

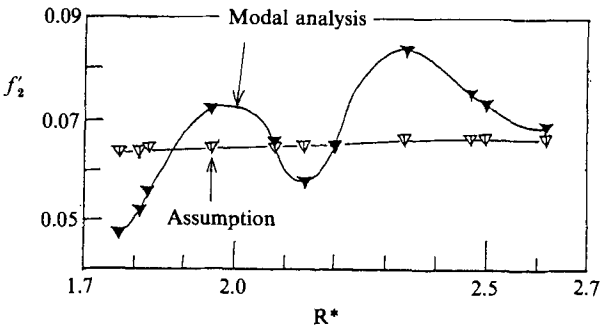

FIGURE 18. Reynolds-number dependence of the modulation frequencies f_2' in the rotating frame computed from (35) and (42), respectively, using the measured values of f_1 and f_2. ▽ and ▼ indicate data computed from (35) (assumption) and (42) (modal analysis), respectively.

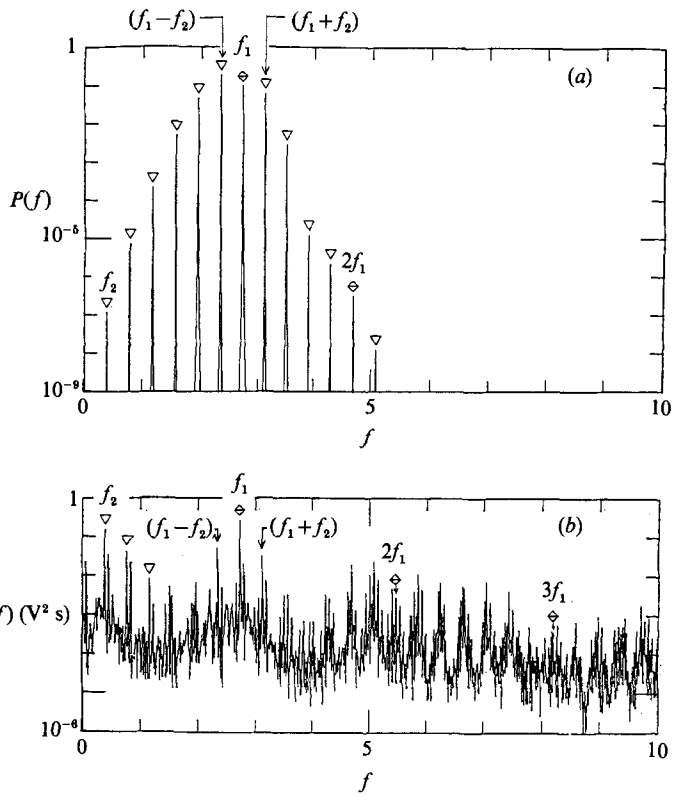

FIGURE 19. Power spectra of the fluctuating colatitude $\tilde{\theta}_{i0}(t,\varphi)$ in the laboratory simulated by (45) and the fluctuating intensity of the laser light scattered by aluminium flakes for the modulated wavy-vortex flow state with $N/m/k = 4/6/-1$ at $R^* = 2.2$. (*a*) Power spectra (arbitrary units) of fluctuating colatitudes $\tilde{\theta}_{i0}(t,\varphi)$ simulated by (45). (*b*) Power spectra of fluctuating intensity (in volts) of scattered light.

figure 12(*a*). A solid line represents a least-square fit of the experimental data to the function (45), where f_1, f_2, k_D and m have the values described in §4.2 and i_{D2} is given in (41); $\varphi = 0$ and

$$\left.\begin{aligned} \bar{a}_{i0} &= 0.933, \quad \hat{a}_{i0} = 0.419, \quad c_{A_{i0}} = 3.73, \\ \bar{w}_{i0} &= 1.33, \quad \hat{w}_{i0} = 1.48, \quad c_{F_{i0}} = 2.19. \end{aligned}\right\} \tag{46}$$

The solid line is in good agreement with the experimental data, as seen in figure 17(*a*). Figure 17(*b*) shows the simulation given by (44), where f_2' has the value described in §4.2, i'_{D2} is given in (36) and the values in (46) are used. The simulation well represents the schematic modulation patterns shown in figure 14.

The modulation frequencies f_2' in the rotating frame computed from both (35) (assumption) and (42) (modal analysis), using the measured values of f_1 and f_2 indicated in figure 16, are shown in figure 18. The difference between the results obtained by the assumption and the modal analysis seems to be caused by assumption (35) or the spectral resolutions $\Delta f/42 = 0.0001$–0.0002 for (35) and $(1+|k|/m)\,\Delta f = 0.006$–$0.012$ for (42).

The power spectra computed from the time series generated by the function (45) are shown in comparison to the scattered-light-intensity power spectra in figure 19. The former were the spectra calculated from the function (45) least-square fitted to the $\tilde{\theta}_j$ fluctuation for $j = \mathrm{i}0$ (solid line in figure 17*a*), which was almost the same as those for other j values. The latter was the spectra obtained from the scattered-light intensity at $\theta = 90°$, which was almost the same as those for other θ-values. Both of the power spectra contain almost the same sharp frequency components, although the relative amplitudes of the components are different.

6. Conclusions

We have considered the unmodulated and modulated travelling azimuthal waves on the toroidal Taylor–Görtler (TG) vortex appearing in the spherical Couette system. These unmodulated and modulated travelling azimuthal waves could be produced with the inner sphere rotating at a specific acceleration rate. We found that the necessary condition for occurrence of the modulation of travelling azimuthal waves is the prevention of spiral TG vortices.

When the wavenumber m is the same, the rotation frequency f_1/m of the travelling azimuthal waves for both wavy and modulated wavy toroidal TG vortex flows shows the same tendency to Reynolds-number dependence as that for the wavy toroidal and spiral TG vortex flow, which can be produced when Reynolds number increases quasi-statically.

Although twelve flow states, m (wavenumber)/k (modulation parameter), are reported in the modulated wavy vortex flow for circular Couette flow, only a state of $6/-1$ is obtained in the present study for spherical Couette flow. The relationship among the characteristic frequencies of modulated travelling azimuthal waves, which is obtained from the modal analysis and the experimental data, is

$$(f_2' + kf_1/m)/f_2 = -1,$$

and is different from the $(f_2' + kf_1/m)/f_2 = 1$ for circular Couette flow, where f_2 and f_2' are modulation frequencies in the laboratory and rotating frames, respectively. The modulated wavy vortex flow includes both amplitude and frequency modulations in spherical as well as circular Couette flow. However, the azimuthal phase angle between amplitude and frequency modulations is different in the two Couette flows; the S-shaped wave is elongated and the flattened wave is shortened, in contrast with the circular-Couette-flow case, in which the S-shaped wave is shortened and the flattened wave is elongated. The magnitude of frequency modulation, $\tilde{t}_{Fj}$, (lengthening and shortening of wavelength) is greater in spherical Couette flow than circular Couette flow. The magnitude of amplitude modulation. $\tilde{A}_j$, (S-shaping and flattening of wave shape) is greater than that of frequency

modulation in spherical Couette flow. The above-mentioned difference in the characteristics of modulated travelling azimuthal waves between spherical and circular Couette flows is caused by the Ekman-boundary-layer effect on the toroidal TG vortices in spherical Couette flow.

The modulated travelling azimuthal waves obtained from the fluctuation in meridian angles of sources and sinks at the vortex boundary were very well simulated by modal analysis of the waves, including not only amplitude modulation but also frequency modulation.

REFERENCES

BARTELS, F. 1982 Taylor vortices between two concentric rotating spheres. *J. Fluid Mech.* **119**, 1.

BOUABDALLAH, A. & COGNET, G. 1980 Laminar–turbulent transition in Taylor–Couette flow. In *Laminar–Turbulent Transition* (ed. R. Eppler & H. Pasel), p. 368. Springer.

BÜHLER, K. & ZIEREP, J. 1983 Transition to turbulence in a spherical gap. In *Proc. 4th Intl Symp. on Turbulent shear flows, Karlsruhe* (ed. L. J. S. Bradbury, F. Durst, B. G. Launder, F. W. Schmidt & J. H. Whitelaw). Springer.

BÜHLER, K. & ZIEREP, J. 1984 New secondary flow instabilities for high Re-number flow between two rotating spheres. In *Laminar–Turbulent Transition* (ed. V. V. Kozlov), p. 677. Springer.

COLES, D. 1965 Transition in circular Couette flow. *J. Fluid Mech.* **21**, 385.

DENNIS, S. C. R. & QUARTAPELLE, L. 1984 Finite difference solution to the flow between two rotating spheres. *Computers and Fluids* **12**, 77.

DIPRIMA, R. C. & SWINNEY, H. L. 1981 Instabilities and transition in flow between concentric rotating cylinders. In *Hydrodynamic Instabilities and the Transition to Turbulence* (ed. H. L. Swinney & J. P. Gollub), p. 139. Springer.

FENSTERMACHER, P. R., SWINNEY, H. L. & GOLLUB, J. P. 1979 Dynamical instabilities and the transition to chaotic Taylor vortex flow. *J. Fluid Mech.* **94**, 103.

GORMAN, M. & SWINNEY, H. L. 1982 Spatial and temporal characteristics of modulated waves in the circular Couette system. *J. Fluid Mech.* **117**, 123.

KING, G. P., LI, Y., LEE, W. & SWINNEY, H. L. 1984 Wave speeds in wavy Taylor-vortex flow. *J. Fluid Mech.* **141**, 365.

KRAUSE, E. 1980 Taylor–Görtler vortices in spherical gaps. *Comp. Fluid Dyn.* **2**, 81.

MOBBS, F. R., PRESTON, S. & OZOGAN, M. S. 1979 An experimental investigation of Taylor vortex waves. In *Taylor Vortex Flow Working Party, Leeds*, p. 53.

MUNSON, B. R. & MENGUTURK, M. 1975 Viscous incompressible flow between concentric rotating spheres. Part 3. Linear stability and experiments. *J. Fluid Mech.* **69**, 705.

NAKABAYASHI, K. 1978 Frictional moment of flow between two concentric spheres, one of which rotates. *Trans. ASME* I: *J. Fluids Engng* **100**, 281.

NAKABAYASHI, K. 1983 Transition of Taylor–Görtler vortex flow in spherical Couette flow. *J. Fluid Mech.* **132**, 209.

NAKABAYASHI, K. & TSUCHIDA, Y. 1988 Spectral study of the laminar–turbulent transition in spherical Couette flow. *J. Fluid Mech.* **194**, 101.

OHJI, M., SHIONOYA, S. & AMAGAI, K. 1986 A note on modulated wavy disturbances to circular Couette flow. *J. Phys. Soc. Japan* **55**, 1032.

RAND, D. 1981 Dynamics and symmetry, predictions for modulated waves in rotating fluids. *Arch. Rat. Mech. Anal.* **79**, 1.

SAWATZKI, O. & ZIEREP, J. 1970 Das Stromfeld im Spalt zwischen zwei konzentrischen Kugelflächen, von denen die innere rotiert. *Acta Mech.* **9**, 13.

SCHRAUF, G. 1986 The first instability in spherical Taylor–Couette flow. *J. Fluid Mech.* **166**, 287.

SCHRAUF, G. & KRAUSE, E. 1984 Symmetric and asymmetric Taylor vortices in a spherical gap. In *Laminar–Turbulent Transition* (ed. V. V. Kozlov), p. 659. Springer.

SWIFT, J., GORMAN, M. & SWINNEY, H. L. 1982 Modulated wavy vortex flow in laboratory and rotating reference frames. *Phys. Lett.* **87 A**, 457.

WAKED, A. M. & MUNSON, B. R. 1978 Laminar–turbulent flow in a spherical annulus. *Trans. ASME* I: *J. Fluids Engng* **100**, 281.

WALDEN, R. W. & DONNELLY, R. J. 1979 Re-emergent order of chaotic circular Couette flow. *Phys. Rev. Lett.* **42**, 301.

WIMMER, M. 1976 Experiments on a viscous fluid flow between concentric rotating spheres. *J. Fluid Mech.* **78**, 317.

YAVORSKAYA, I. M., BELYAEV, YU. N., MONAKHOV, A. A., ASTAF'EVA. N. M., SCHERBAKOV, S. A. & VVEDENSKAYA, N. D. 1980 Stability, nonuniqueness and transition to turbulence in the flow between two rotating spheres. *Rep.* 595. Space Research Institute of the Academy of Science, USSR.